EuroSun2026

OPTICAL ANALYSIS OF A SOLAR POLYGENERATION COLLECTOR FOR COMBINED ELECTRICITY, HEAT, HYDROGEN FUEL AND WASTEWATER TREATMENT

Muhammad Talha Jahangir[1], Nathan Blanc[2], Chandan Pandey[2], Christos N. Markides[2], Ivan Acosta-Pazmiño[1,3 *]
[1]MG Sustainable Engineering AB, 753 21 Uppsala, Sweden
[2]Clean Energy Processes (CEP) Laboratory, Department of Chemical Engineering, Imperial College London, London, SW7 2AZ, UK
[3]Department of Building Engineering, University of Gävle, 801 76 Gävle, Sweden
[*] ivan@mgsust.com

Summary

The growing need for the decarbonisation of industry and the transition to renewable energy calls for more efficient utilisation of available solar resource than conventional solar technologies. One pathway to this goal is implementing poly-generators: combined units for generating electricity, heat, and additional vectors. Herein, we present an analysis of a solar collector that integrates water treatment with heat, electricity, and hydrogen generation. Selected parts of the solar spectrum are utilised for different purposes to enhance the total exergy efficiency of the collector. In this study optical performance curves for 3 different configurations are presented, discussed and compared for a low concentrating solar collector. The single-channel spectral-splitting configuration reaches an optical efficiency above 75% at normal incidence, against below 65% for the two-channel configuration, and was selected for the subsequent analysis on that basis; the tube-array configuration performs almost identically. East–west positioning is preferable because optical efficiency stays essentially constant up to about 70° incidence, whereas in the north–south plane it declines from about 30°. For the selected configuration, the photocatalytic reactor receives 643 W/m², the PV cells 557 W/m² and the thermal absorber 1369 W/m², and the choice of working fluid changes the irradiance on the cells by less than 20% (557, 457 and 450 W/m² for pure water, the SiO_2–Ag nanofluid and the water–glycerol solution).

PV-T, Spectral splitting, Green hydrogen, Photocatalysis, Solar water-treatment

Field of application for the findings: Photovoltaic, solar-thermal plants, Hydrogen generation, Solar industry

Addressed audience: industry, academia

---

1. Introduction

Solar collectors are normally built to deliver a single energy vector, either electricity or heat, and each converts well only the part of the spectrum that suits that vector; the remainder is lost or degraded to low-grade heat. Polygeneration uses the same aperture more effectively. By matching each spectral band to the conversion process best suited to its photon energy, a single collector can deliver electricity, heat, and a chemical fuel from the same incident radiation, increasing useful output and exergy efficiency per unit collector area. This is relevant for industry, which accounts for a significant share of energy consumption and environmental pollution in the European Union (Procházková et al., 2023) and where decarbonising energy demand is central to national and international energy policy (IEA, 2023). Roof and yard area at industrial sites is limited, so the value of a collector is set by what it delivers per square metre rather than by any single efficiency. This type of collector can also treat an industrial wastewater stream while generating hydrogen, turning a waste flow into a resource; wastewater reuse in Europe remains low owing to regulatory, technological, and economic barriers (Malinauskaite et al., 2024). Aligned with the Paris Agreement goal of limiting global temperature rise to below 2 °C compared to pre-industrial levels, the EU has committed to becoming the first climate-neutral continent by 2050, and through initiatives such as the European Green Deal it is accelerating the deployment of clean energy technologies (Bäckstrand, 2022).

This work is carried out within the SPECTRUM project, which develops a solar concentrating collector that cogenerates heat, electricity, and hydrogen through a cascade-like conversion of concentrated sunlight (SPECTRUM, 2026). By matching the energy grade of each spectral band to a conversion process, the system uses ultraviolet (UV) light for photocatalytic hydrogen production with simultaneous pollutant degradation, the infrared (IR) band for thermal energy, and the visible and near-infrared (VIS/NIR) band for photovoltaic electricity generation. Depending on the location and type of the spectral splitter, it could potentially thermally decouple the PV cells from the thermal absorber, enabling higher-temperature heat generation without compromising electrical efficiency. Two collector prototypes are being developed within the project, a low-temperature collector (SPECTRUM-LT) and a high-temperature collector (SPECTRUM-HT); targeting up to 100°C and 200°C at the fluid outlet, respectively, this paper concerns the optical design of the former.

Compared with conventional photovoltaic–thermal (PVT) collectors, the optical design of such a poly-generator raises three challenges. First, the device has multiple outputs to optimise for, and the appropriate balance between electricity, hydrogen, and heat depends partly on metrics that are not strictly technical; the optical design must therefore provide a reasonable division of the incident radiation between the spectral splitter, the photocatalytic filter, and the PV cells rather than optimise a single objective. Second, the additional optical components introduce additional losses, which must be kept to a minimum if the design is to be competitive with established PVT systems or standalone solutions. Third, the design space contains more degrees of freedom than for classical PVT collectors, since the geometry and the optical properties of every component can be varied.

Conventional photovoltaic–thermal (PVT) collectors, which co-generate heat and electricity from a shared aperture, are an established technology with a broad literature covering collector types, absorber concepts, and system integration (Herrando et al., 2023). The poly-generator extends this proven co-generation idea by two further vectors, hydrogen and treated wastewater. Both added pillars of the concept are, in turn, established individually. Spectral beam splitting for hybrid solar converters has been reviewed extensively, from the early filter- and mirror-based concepts (Imenes and Mills, 2004) to concentrated photovoltaic–thermal systems in which liquid absorptive filters, dichroic mirrors, and selective absorbers divide the spectrum between PV cells and thermal receivers (Ju et al., 2017). On the photochemical side, dual-functional photocatalysis, in which hydrogen evolution is combined with the simultaneous degradation of organic pollutants acting as sacrificial agents, has developed into an active research field (Bi et al., 2026). The poly-generator considered here combines the two approaches in a single collector and adds a third energy vector, low-temperature heat, which distinguishes it from the two-output systems covered by these reviews.

Herein, we present an optical analysis of a polygeneration solar collector for heat, electricity and hydrogen fuel, where the latter is achieved via photocatalytic water treatment. A general schematic of the collector is presented in Fig. 1. Irradiance is concentrated and split into IR radiation, which is used for heating a heat transfer fluid (HTF); UV radiation, which is used for photocatalytic wastewater remediation, generating hydrogen in the process; and visible and near-IR radiation, which is used for photovoltaic electricity generation. Fig. 2 presents the solar spectrum and approximate cut-off wavelengths. Exact cut-in wavelengths will be determined during the design process through material selection for various components of the poly-generator. The upper bound of the photovoltaic band is set by the spectral response of the crystalline silicon cells, which falls to zero at the band edge near 1100 nm; radiation beyond that wavelength cannot be converted by the cells and is available as heat. The spectral split occurs as the photocatalytic reactor captures UV rays while allowing visible and IR radiation to pass through to the PV, which is ultimately cooled by the thermal absorber.

The objectives of this paper are threefold: (i) to document the optical simulation methodology in sufficient detail to be reproducible; (ii) to compare the optical performance of three candidate channel configurations for the PCR under varying incidence angles and working fluids; and (iii) to select the configuration carried forward to the thermal design and to quantify the irradiance reaching each component of the receiver. The resulting design forms the basis of the subsequent thermal analysis of the collector. Section 2 describes the collector concept and configurations, Section 3 the optical model, and Section 4 the results; Section 5 discusses the model assumptions and their implications, and Section 6 concludes.

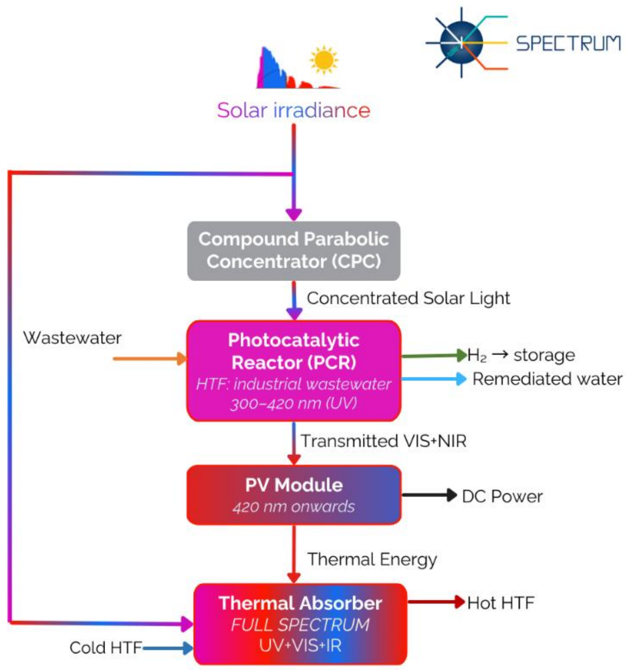

Fig. 1: Cascade conversion in the SPECTRUM low-temperature collector

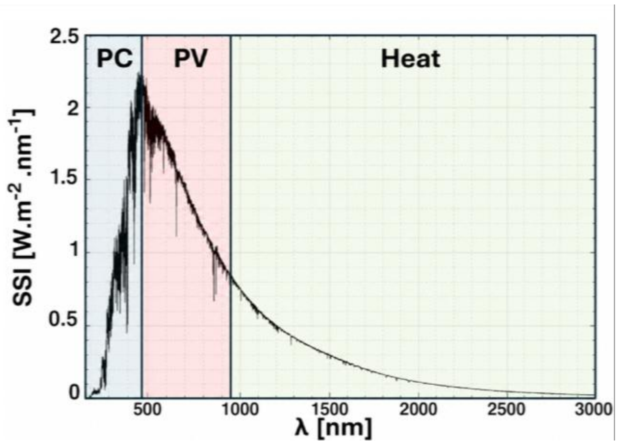

Fig. 2: The AM1.5 solar spectrum divided into the bands used for photocatalysis (PC), photovoltaic conversion (PV) and heat, where SSI denotes the spectral solar irradiance. The upper limit of the PV band corresponds to the spectral response of the crystalline silicon cells, which cuts off near 1100 nm.

2. The poly-generation collector

2.1. Collector configuration

Fig. 2 shows the general schematic of the collector. It includes a glass cover to reduce convective losses, a Double MaReCo (Solarus) concentrator to achieve a concentration ratio of 1.3, and a generator apparatus, which is the heart of the system. Three configurations are considered: the single-channel configuration, the two-channel configuration, and the tube array. The first configuration, known as the single-channel configuration, uses a single filter channel, with the thermal absorber integrated into the PV modules. In this configuration, the cooling channels of the PV modules also serve as the thermal absorber. In contrast, the two-channel configuration includes a separate thermal absorber channel. This allows the absorber water to be heated for thermal utilisation without heating the PV module, maintaining separate optimal temperatures (one for high-efficiency PV and another for heat utilisation). The third configuration is also single-channel, with the absorber integrated into the PV module. However, the filter channel is replaced by a more realistic tube array.

The three configurations embody different trade-offs. The single-channel arrangement is mechanically the simplest, but it couples the PV operating temperature to the heat delivery temperature, since the same channels cool the cells and carry the thermal output. The two-channel arrangement decouples these temperatures, which is attractive thermodynamically, but the additional channel and its interfaces penalise the optics, as quantified in Section 4. The tube array replaces the idealised rectangular filter channel with a geometry closer to a manufacturable reactor. Which of these trade-offs dominates is an optical question, and this paper aims to answer it through the comparison presented.

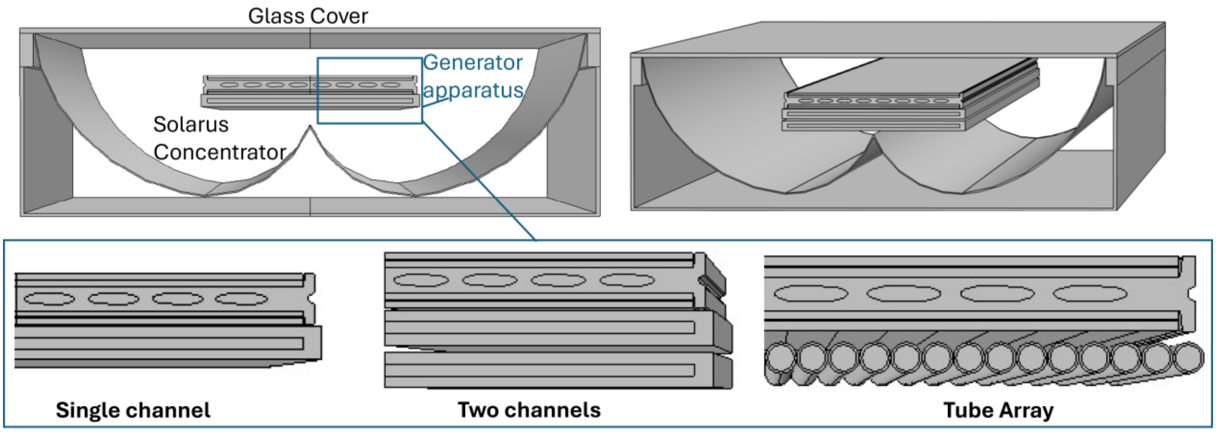

Fig. 2: Detailed description of the poly-generator, including the solar concentrator and the generator apparatus in three configurations: a single-channel configuration where the thermal absorber is integrated within the PV module, a two-channel configuration with a separate photocatalytic channel and thermal channel, and a tube-array configuration.

2.2. Selection of the concentrator

The concentrator is based on the Double-MaReCo (Solarus Power Collector) and employs a symmetric, truncated compound parabolic concentrator (CPC) geometry with a transverse bifacial photovoltaic–thermal receiver. In the literature, this configuration is classified as a low-concentrating PVT (LCPVT) collector. The concept has been extensively optimised and studied, most notably by Cabral et al. (2019), who combined Monte Carlo ray tracing, electrical modelling, and ISO 9806:2017-based thermal modelling to analyse optical efficiency, incidence-angle modifiers, irradiance uniformity, shading effects, and annual energy yields. That study identified the CPC-2 geometry as the most promising configuration owing to its higher annual electrical and thermal energy yield, improved irradiance uniformity on the bifacial receiver, and reduced sensitivity to partial shading, making it particularly well suited for stationary collectors without tracking. This geometry is adopted here as the optical basis of the low-temperature poly-generator.

The choice of a stationary, low-concentrating geometry keeps the concentration ratio modest (1.3) but avoids tracking hardware, which suits roof-mounted installations at industrial sites and reduces CAPEX and OPEX for the solar field based on such a collector.

2.3. Operating principle of the receiver stack

Within the collector, the concentrated radiation is divided by the spectral splitting/filtering arrangement (Fig. 1). The UV, visible, and near-infrared fractions enter the photocatalytic reactor (PCR) channel, where the wastewater stream absorbs the UV light and the photocatalyst drives simultaneous pollutant remediation and hydrogen evolution; the produced hydrogen is routed to purification and storage. The visible and near-infrared radiation transmitted by the reactor reaches the PV cells for electricity generation. The infrared fraction not harvested by the PV is recovered as heat by the thermal absorber, which heats the incoming heat-transfer fluid, which leaves the collector as the hot stream. In the low-temperature collector investigated here, the reactor channel itself acts as the spectral filter, and the thermal absorber is integrated with the PV modules as described in Section 2.1. Fig. 4 shows the resulting receiver stack together with the material of each component and the spectral band assigned to it: the photocatalytic reactor carries the industrial wastewater and takes the 300–420 nm band, the silicon cells with their EVA encapsulation convert the band from 420 nm onwards, and the aluminium thermal absorber, which receives the remaining spectrum, carries the water heat-transfer fluid. A low-emissivity coating limits the radiative loss from the absorber, and the aluminium concentrator and the wooden case complete the assembly.

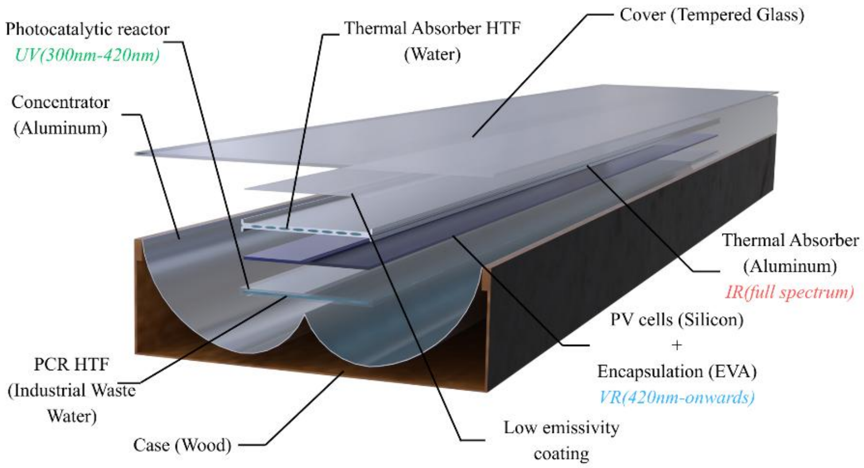

Fig. 4: Cut-away view of the low-temperature receiver, showing each component, its material and the spectral band assigned to it: the photocatalytic reactor carrying the industrial wastewater (300–420 nm), the silicon PV cells with EVA encapsulation (420 nm onwards), and the aluminium thermal absorber carrying the water heat-transfer fluid (remaining spectrum). The tempered-glass cover, aluminium concentrator, low-emissivity coating, and wooden case are also indicated.

3. Methodology

3.1. Optical model and assumptions

The optical model was developed in COMSOL Multiphysics using the ray optics module to evaluate the optical performance of the polygenerating collector. Three simplifying assumptions are made. First, incident solar radiation consists of parallel rays, with the finite angular diameter of the solar disc neglected. Second, surface roughness effects are ignored; all surfaces are treated as perfectly smooth, eliminating scattering phenomena. Third, all optical materials are assumed to be completely homogeneous. The incoming radiation first crosses the cover glass of the collector, then reflects off the parabolic trough concentrator towards the generator apparatus with a constant reflectance of 95%. Finally, it enters the photocatalytic reactor channel, which acts as the spectral splitter, absorbing the UV part of the spectrum before reaching the cells. The filter channel walls are assumed to have a transmissivity of 90%, while the transmissivity of water is calculated from transmissivity data. Of the radiation reaching the cells, only a fraction is converted into electricity, while the remainder is converted into thermal energy. The parameters of the optical model are summarised in Tab. 1. Each simulation released approximately 3,000 rays, and their trajectories and the flux arriving at every surface were recorded. The spectral dependence is taken into consideration based on the transmittance of the filter, so no discretisation of the solar spectrum into wavelength bands was employed. The spectral irradiance reaching the photovoltaic cells is expressed by eq. 1

$$G_{pv}(\lambda) = G_{AM1.5}(\lambda) \cdot \rho_c \cdot \tau_g \cdot \tau_{fl}(\lambda) \qquad \text{(eq. 1)}$$

where $G_{AM1.5}(\lambda)$ is the incident solar spectral irradiance, $G_{pv}(\lambda)$ the spectral irradiance received by the cells, ρ_c the concentrator reflectivity, τ_g the glass transmittance, and $\tau_{fl}(\lambda)$ the wavelength-dependent filter transmittance. Equation 1 describes the concentrated path that reaches the lower face of the bifacial receiver. The upper face is illuminated directly through the cover glass without striking the concentrator, so ρc does not apply; the two contributions are treated separately when the irradiance on each receiver component is evaluated in Section 5.

Tab. 1: Optical and simulation parameters of the ray-tracing model.

Parameter	Value	Source/note
Concentrator geometry	symmetric truncated CPC (Double MaReCo)	Cabral et al. (2019)
Concentrator reflectance ρ_c	0.95	constant, wavelength-independent
Cover glass transmittance τ_g	0.90	clean conditions
Filter transmittance $\tau_{fl}(\lambda)$	0.90 (clean), fluid-dependent	measured / COMSOL database

Reference spectrum	AM1.5G	standard test spectrum
Rays released per simulation	≈ 3,000	ray optics module
Spectral treatment	wavelength-dependent filter transmittance	no discretisation into bands
Incidence angles simulated	0–90°, north–south and east–west planes	stationary collector
Assumed PV conversion efficiency	20%	Used to derive absorber irradiance

The optical simulation determines the spatial distribution of the flux incident on the filter and on the primary PVT channel; these locally varying flux values are circumferentially averaged and applied as uniform heat-flux boundary conditions in the subsequent CFD analysis. For each configuration and incidence angle, the simulation yields the ray paths, the flux distributions on the receiver surfaces, and the fraction of the released radiative power intercepted by each component, from which the optical efficiency is evaluated.

3.2. Working fluids

Because the working fluid for the photocatalytic channel has not yet been selected, three candidate fluids were considered: pure water, a SiO_2–Ag nanofluid, and a water–glycerol solution with a concentration of 0.075 M containing a photocatalyst, as investigated experimentally within the project. The spectral transmittance of a 3 mm layer of each fluid is shown in Fig. 5. The optical properties of water and of the SiO_2–Ag nanofluid were taken from the COMSOL material database, while the data for the water–glycerol solution were interpolated from unpublished experimental measurements provided by the project partners. The effect of the nanoparticles is mostly evident at shorter wavelengths, whereas glycerol reduces the transmission across the entire spectrum. Section 4.4 discusses the influence of these optical properties on PV cell irradiation.

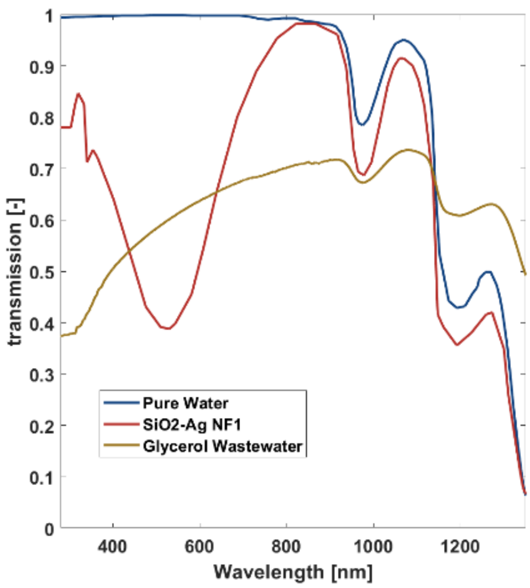

Fig. 5: Spectral transmittance of the three candidate working fluids (3 mm layer): pure water, SiO_2–Ag nanofluid, and water–glycerol solution with photocatalyst.

4. Results

4.1. Ray trajectories

Ray trajectories from a typical simulation are presented in Fig. 6. To improve visibility, only 300 of the simulated rays are shown. As shown, the concentrator works well, directing most rays toward the generator apparatus. Some rays are deflected by the sides, and others are not reflected due to the imperfect reflectance of the concentrator. The three-dimensional view (left) shows the ray paths along the trough, while the transverse cross-section (right) shows the reflected rays converging from both parabolic wings onto the underside of the receiver, illustrating the bifacial illumination provided by the concentrator.

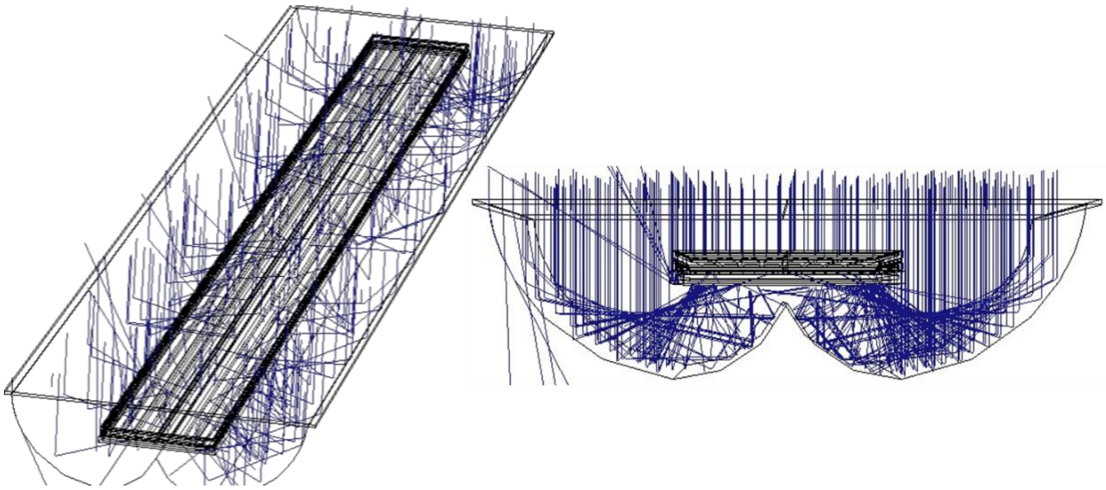

Fig. 6: Ray trajectories from the simulation results; 300 of the simulated rays are shown for clarity.

4.2. Radiation distribution on the receiver

Fig. 7 presents the radiation distribution on the top and bottom surfaces of the receiver for the different configurations. For improved visibility, the profiles are smoothed. The concentrated radiation on the bottom surface is mostly focused along two focal lines, consistent with the ray trajectories in Fig. 6. The top surface receives the unconcentrated direct irradiance and is therefore comparatively uniform, whereas the bottom surface collects the reflected, concentrated radiation from the two parabolic wings. The patchy character of the distribution is a numerical artefact of the discrete rays used in the optical simulation rather than a physical feature. The averaged profiles from Fig. 7 were used to calculate the optical efficiency and the irradiance delivered to each receiver component, discussed in Section 5.

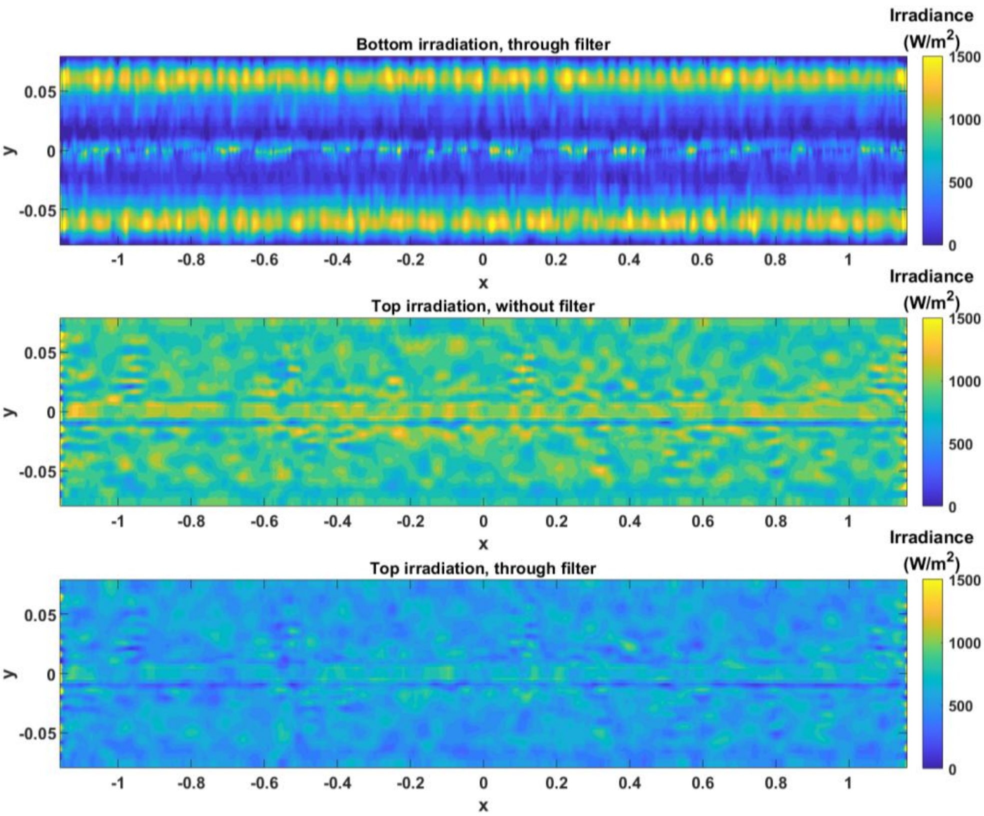

Fig. 7: Radiation profile on the top and bottom surfaces of the solar collector with different configurations.

4.3. Optical efficiency and incidence-angle response

Fig. 8 presents the optical efficiency of the three configurations as a function of incidence angle for incidence-angle variation in the north–south and east–west planes. For all three configurations, the optical efficiency lies between 65% and 75% at normal incidence (0°) and drops to very low values above 70° in both planes. In the east–west plane, the efficiency remains very stable up to this critical angle, with no significant drop, whereas in the north–south plane the deterioration begins earlier, with a noticeable decline already at incidence angles around 30°. The east–west positioning is therefore preferable: the optical efficiency stays essentially constant over the wide range of incidence angles swept during a day, whereas the north–south positioning loses a substantial part of the collected radiation well before the acceptance limit is reached. This behaviour matters because the collector, like the underlying MaReCo design, is intended for stationary installation without tracking, so the optical efficiency at non-zero incidence angles directly shapes the daily and seasonal energy yield.

In both planes, the two-channel and single-channel configurations differ significantly in optical efficiency. At normal incidence, the single-channel configuration achieves an efficiency above 75%, compared with below 65% for the two-channel configuration, and this gap persists over the whole range of incidence angles. The two-channel configuration was therefore rejected, and the single-channel configuration was selected for the subsequent thermal analysis based on its superior optical efficiency. The optical efficiency of the tube-array configuration is nearly identical to that of the single-channel configuration, which indicates that the remaining simulations can be performed with either geometry without a significant loss of accuracy; the single-channel geometry was retained because it is simpler and less prone to numerical divergence.

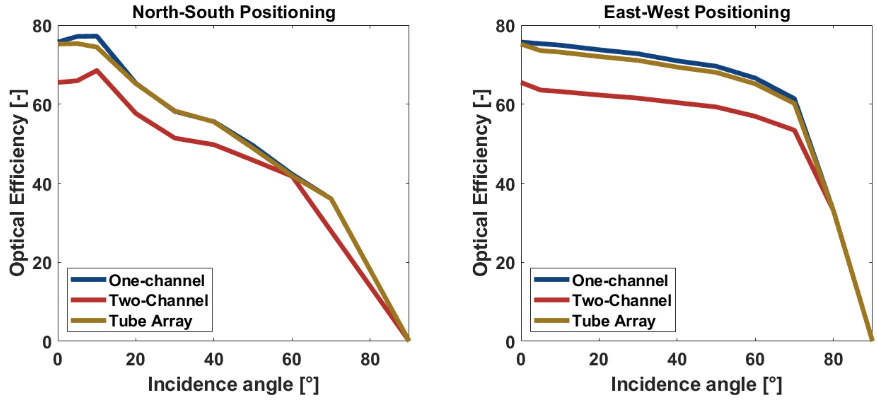

Fig. 8: Optical efficiency of the different configurations vs. incidence angle, in the north–south (left) and east–west (right) planes.

4.4. Effect of the working fluid

Based on the transmittances of the fluids and surfaces, the irradiation distribution within the visible range on the PV cells was calculated for the three candidate working fluids (Fig. 9). The distributions follow similar trends, with the presence of glycerol affecting the total irradiation most strongly: the average irradiance on the PV cells is 557 W/m² for pure water, 457 W/m² for the SiO_2–Ag nanofluid, and 450 W/m² for the water–glycerol solution. In this total-power analysis, the difference is not significant enough to warrant a change in the optical design. The similar behaviour of the water–glycerol solution and the SiO_2–Ag nanofluid indicates that different waste streams may behave similarly; this conclusion should be validated when data for additional types of wastewater become available.

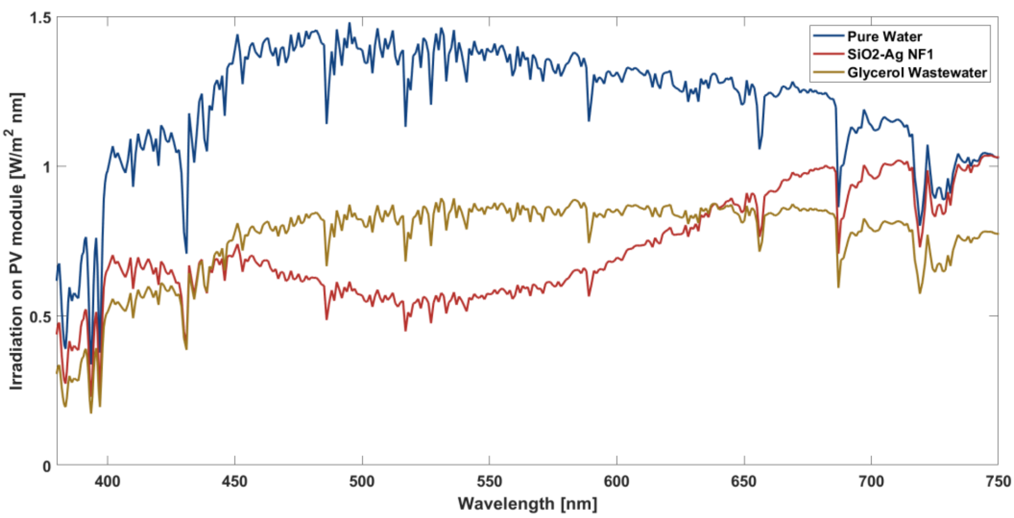

Fig. 9: Effect of the fluid properties on the irradiation of the PV cells for the three candidate working fluids.

5. Discussion

The averaged radiation profiles of Fig. 7 also give the irradiance delivered to each component of the receiver for the selected single-channel configuration: the irradiance on the bottom surface without the filter corresponds to the photoreactor; the irradiance on the bottom surface transmitted through the filter corresponds to the PV cells; and the irradiance on the thermal absorber is obtained by subtracting the fraction converted to electricity (assuming a PV efficiency of 20%) from the bottom irradiance and adding the irradiance on the top surface, so that heat collected on both sides of the bifacial receiver is accounted for. On this basis, the photoreactor receives 643 W/m², the PV cells 557 W/m² and the thermal absorber 1369 W/m². These values are the input to the thermal design of the collector, and they show that the cascade arrangement leaves a useful irradiance for all three conversion processes rather than favouring one at the expense of the others.

The optical model involves idealisations whose effect on the reported values should be kept in mind. Solar radiation is modelled as parallel rays, so the finite angular size of the solar disc and circumsolar radiation are neglected; in reality, the transition at the acceptance limit will be smoother than the sharp drop seen in Fig. 6. All surfaces are treated as smooth and all materials as homogeneous, which excludes scattering losses, and the transmittances of 90% assume clean conditions, so soiling in outdoor operation will reduce the delivered irradiances below the values reported here. The concentrator reflectance is taken as a constant 95%, independent of wavelength and incidence angle. These assumptions are conventional at the design stage, but they should be revisited when the experimental prototypes are characterised.

The optical efficiency of 75% at normal incidence is lower than the values reported for the Double MaReCo concentrator in its conventional PVT use, which is attributed to the larger receiver apparatus of the poly-generator: the additional filter channel increases the width of the receiver and thereby the fraction of reflected rays that miss it or are intercepted more than once. Recovering part of this difference is a geometric task for the detailed design, through refining the receiver dimensions relative to the concentrator and reducing the interface losses of the cover glass and the filter channel.

The working-fluid comparison indicates that the optical design is robust to the final fluid selection: replacing pure water with the SiO_2–Ag nanofluid or the water–glycerol solution reduces the average PV irradiance by approximately 18% and 19%, respectively, which was not considered sufficient to alter the design at this stage. The fluid can therefore be selected primarily on the basis of its photocatalytic performance, with the optical consequences accounted for in the subsequent electrical yield analysis. The selected single-channel model now provides the boundary conditions for the thermal design of the collector, and the equivalent analysis of the high-temperature collector will complete the optical design of the SPECTRUM concept.

6. Conclusion

A novel concept for the combined generation of electricity, heat, and hydrogen fuel with integrated wastewater treatment was presented, and its optical design was analysed using a multi-physics simulation approach. With respect to the objectives set in the introduction, the simulation methodology and its assumptions were documented (i), the three candidate configurations were compared under varying incidence angles and working fluids (ii), and the configuration carried forward to the thermal design was selected (iii). The two-channel configuration was rejected because its optical efficiency was below 65% at normal incidence, compared with more than 75% for the single-channel configuration. The near-identical performance of the tube-array and single-channel configurations means the simpler, numerically more stable single-channel geometry can represent the collector in further simulations.

East–west positioning is preferable, since optical efficiency remains essentially constant up to the acceptance limit, whereas in the north–south plane it declines from incidence angles of about 30°. For the selected design, the photoreactor receives 643 W/m², the PV cells 557 W/m² and the thermal absorber 1369 W/m². The influence of the working fluid on PV irradiation was modest (557, 457, and 450 W/m² for pure water, the SiO_2–Ag nanofluid, and the water–glycerol solution, respectively) and does not warrant a design change at this stage. The selected optical design forms the basis for the thermal design of the low-temperature collector. Future work within the SPECTRUM project includes the optical design of the high-temperature collector, the integration of experimentally characterised wastewater streams, and the construction and outdoor testing of the prototypes.

7. Acknowledgement

This work has been developed under the framework of the SPECTRUM project, funded by the European Union under the Horizon Europe research and innovation programme, topic HORIZON-CL5-2024-D3-01-10 (Research and Innovation Action, grant agreement no. 101172891). The authors thank the SPECTRUM project partners for providing the experimental transmittance data for the water–glycerol solution, and their colleagues at LNEG (Laboratório Nacional de Energia e Geologia) and Fraunhofer ISE for their constant support and valuable discussions throughout this work.

8. References

Bäckstrand, K., 2022. Towards a climate-neutral union by 2050? The European Green Deal, climate law, and green recovery, in: Bakardjieva Engelbrekt, A., Ekman, P., Michalski, A., Oxelheim, L. (Eds.), Routes to a Resilient European Union. Palgrave Macmillan, Cham. https://doi.org/10.1007/978-3-030-93165-0_3

Bi, H., Yang, G., Liu, Q., Zhao, R., Chen, F., Shen, Z., 2026. Synergistic dual-functional photocatalysis for hydrogen production simultaneously with pollutant degradation and value-added compound production. Chinese Chemical Letters, 112463. https://doi.org/10.1016/j.cclet.2026.112463

Cabral, D., Gomes, J., Karlsson, B., 2019. Performance evaluation of non-uniform illumination on a transverse bifacial PVT receiver in combination with a CPC geometry. Solar Energy 194, 696–708. https://doi.org/10.1016/j.solener.2019.10.069

Herrando, M., Wang, K., Huang, G., Otanicar, T., Bany Mousa, O., Agathokleous, R.A., Ding, Y., Kalogirou, S., Ekins-Daukes, N., Taylor, R.A., Markides, C.N., 2023. A review of solar hybrid photovoltaic-thermal (PV-T) collectors and systems. Progress in Energy and Combustion Science 97, 101072. https://doi.org/10.1016/j.pecs.2023.101072

IEA, 2023. Australia 2023: Energy Policy Review. International Energy Agency, Paris.

Imenes, A.G., Mills, D.R., 2004. Spectral beam splitting technology for increased conversion efficiency in solar concentrating systems: a review. Solar Energy Materials and Solar Cells 84, 19–69. https://doi.org/10.1016/j.solmat.2004.01.038

Ju, X., Xu, C., Han, X., Du, X., Wei, G., Yang, Y., 2017. A review of the concentrated photovoltaic/thermal (CPVT) hybrid solar systems based on the spectral beam splitting technology. Applied Energy 187, 534–563. https://doi.org/10.1016/j.apenergy.2016.11.087

Malinauskaite, J., Delpech, B., Montorsi, L., Venturelli, M., Gernjak, W., Abily, M., Stepišnik Perdih, T., Nyktari, E., Jouhara, H., 2024. Wastewater reuse in the EU and Southern European countries: policies, barriers and good practices. Sustainability 16 (24), 11277. https://doi.org/10.3390/su162411277

Procházková, M., Touš, M., Horňák, D., Miklas, V., Vondra, M., Máša, V., 2023. Industrial wastewater in the context of European Union water reuse legislation and goals. Journal of Cleaner Production 426, 139037. https://doi.org/10.1016/j.jclepro.2023.139037

SPECTRUM, 2026. Solar polygeneration collector for combined heat, power, hydrogen fuel and wastewater treatment. Horizon Europe project no. 101172891. https://doi.org/10.3030/101172891 (accessed 16 July 2026).